Diabetes Publish Ahead of Print, published online December 10, 2009

A Central Role of RLIP76 in Regulation of Glycemic Control

Running Title: Mechanisms of Insulin Resistance

Sanjay Awasthi*, Sharad S. Singhal, Sushma Yadav, Jyotsana Singhal, Rit Vatsyayan, Ewa Zajac, Rafal Luchowski, Jozef Borvak, Karol Gryczynski, Yogesh C. Awasthi

Department of Molecular Biology & Immunology, University of North Texas Health Science Center, Fort Worth, TX 76107

***Address correspondence to:**
Sanjay Awasthi, M.D.,
Email: ssinghal@hsc.unt.edu

Submitted 19 June 2009 and accepted 25 November 2009.

Objective: Pathology associated with oxidative stress frequently result in insulin-resistance. Glutathione (GSH) and GSH-linked metabolism is a primary defense against oxidative stress. Electrophilic lipid-alkenals, such as 4-HNE, generated during oxidative stress are metabolized primarily to GSH-conjugates (GS-E). Recent studies show that RLIP76 is the primary GS-E transporter in cells, and a regulator of oxidative-stress response. Because $RLIP76^{-/-}$ mice are hypoglycemic, we studied the role of RLIP76 in insulin-resistance.

Research Design and Methods: BG, insulin, lipid measurements and hyperinsulinemic-euglycemic and hyperglycemic clamp experiments were performed in $RLIP76^{+/+}$ and $RLIP76^{-/-}$ C57B mice, using IACUC approved protocols. Time-resolved 3-D confocal fluorescence microscopy was used to study insulin-endocytosis.

Results: The plasma insulin/glucose ratio was ordered $RLIP76^{-/-}$ < $RLIP76^{+/-}$ < $RLIP76^{+/+}$; administration of purified RLIP76 in proteoliposomes to $RLIP76^{+/+}$ animals further increased in this ratio. RLIP76 was induced by oxidative or hyperglycemic-stress; the concomitant increase in insulin-endocytosis was completely abrogated by inhibiting the transport activity of RLIP76. Hydrocortisone could transiently correct hypoglycemia in $RLIP76^{-/-}$ animals, despite inhibited activity of key glucocorticoid-regulated hepatic gluconeogenic enzymes, PEPCK, G-6-Pase and F-1,6-BP, in $RLIP76^{-/-}$.

Conclusions: The GS-E conjugate transport activity of RLIP76 mediates insulin-resistance by enhancing the rate of clathrin-dependent endocytosis of insulin. Because RLIP76 is induced by oxidative stress, it could play a role in insulin-resistance seen in pathological conditions characterized by increased oxidative stress.

Oxidative stress is implicated in chronic diseases (1-4) including insulin resistance that leads to type II diabetes mellitus (5-8). Pancreatic β-cells are relatively susceptible to the damaging effects of free radicals because of low levels of free radical quenching enzymes including catalase, glutathione-peroxidase and superoxide dismutase (9). Short exposure of β-cells to H_2O_2 suppresses insulin mRNA levels and insulin secretion (10). Likewise, exposures of β-cells to high glucose concentrations leads to increased intracellular free radicals content and inhibited insulin release (11). ROS generated during oxidative stress are known to activate signaling proteins including stress kinases (e.g. c-Jun N-terminal kinase, p38, IκB kinase), and also the extracellular receptor kinases which can affect the cellular response to insulin. The down-regulation of insulin response under oxidant-exposure involves activation of TNFα; increased Ser/Thr phosphorylation of insulin receptor and insulin receptor substrate-1 (IRS1) (12, 13) reduces the re-distribution of IRS1 and phosphatidylinositol-kinase (PI3K) from the cytosolic to microsomal fraction, reduces protein kinase-B (Akt) phosphorylation, and results in decreased trafficking of GLUT4 to the plasma membrane. Prolonged exposure to oxidative stress also affects the transcription of glucose transporter GLUT4 (14).

In parallel with the protein signaling pathway described above, a chemical signaling pathway is activated by oxidative stress. This pathway, begins with ROS derived from oxidative degradation of poly-unsaturated fatty acids (PUFA), and is linked with multiple protein signaling pathways. Activation of protein kinase C (PKC) and NFκB results in increased activity of NADPH oxidase (15), which amplifies oxidative stress by augmenting the recycling of Fe^{+++} to Fe^{++} (16). The auto-catalytic chain reaction of lipid peroxidation, where a single lipid peroxide species can lead to the formation of up to a thousand lipid peroxides, provides a built in magnification for ROS mediated signaling. The α, β-unsaturated lipid aldehydes generated through β-scission of linoleic acid, γ-linoleic acid, or arachidonic acid hydroperoxides play an important role in this signaling. 4-hydroxy-*t*-2-nonenal (4HNE), the most abundant alkenals generated in cells, is a versatile second messenger for signaling which can affect multiple signaling pathways including those for apoptosis, differentiation, proliferation, and also the receptor tyrosine-kinase (RTK) mediated signaling (17,18).

4HNE control the expression and activity of many signaling proteins involved in insulin-resistance, including stress-kinases, NFκB and chaperones (19), and affects RTK signaling, thus HNE could modulate insulin signaling and glucose homeostasis. Glutathione transferases (particularly GSTA4-4) and RLIP76 (a 76 kDa splice variant, encoded by the human gene RALBP1) are the two major determinants of 4HNE levels in cells (20). While 4HNE is substrate for several enzymes including aldehyde dehydrogenases, aldose reductase, and Cyt-p450, the major pathway for its disposition from cells is through its GST catalyzed conjugation to GSH (20) and subsequent ATP-dependent transport of the conjugate (GS-HNE) catalyzed by RLIP76 (21). The mechanisms for the efflux of glutathione-electrophiles conjugates (GS-Es) are complex, involving other ABC-transporters, but knockout-mouse studies have shown that RLIP76 plays a dominant role (22, 23). The relevance of RLIP76 to insulin resistance is also suggested by its known function as a component of clathrin-dependent endocytosis (22-26), a determinant of the duration of ligand-receptor signal. Present studies provide evidence for a novel model in which the mechanisms of insulin-resistance are directly linked to mercapturic acid pathway

through the role of RLIP76 as an energy providing component of clathrin-dependent endocytosis. Compelling evidence for this model is presented in this communication.

RESEARCH DESIGN AND METHODS

Quantification of insulin, glucose and lipid levels in wild type and RLIP76 knockout mouse: Animal experiments were carried out in accordance with an IACUC approved protocol. Twelve weeks old C57BL/6 mice born of heterozygous x heterozygous ($RLIP76^{+/-}$ x $RLIP76^{+/-}$) mating were genotyped by PCR strategy on mouse tail DNA using forward, reverse and long terminal region (LTR) primers (27). Insulin and glucose measurement in blood serum were performed on wild-type ($RLIP76^{+/+}$) animals sacrificed 24 h after a single i.p. injection of control or RLIP76-liposomes equivalent to 200 and 500 μg RLIP76 protein. Insulin and glucose measurement in blood serum were also performed on heterozygous ($RLIP76^{+/-}$) and homozygous ($RLIP76^{-/-}$) animals. Cholesterol, triglycerides, glucose and insulin measurements were re-assayed and verified in the laboratory of Dr. Kent R. Refsal, Michigan State University, Michigan. Uptake of RLIP76 by tissues of RLIP76 proteoliposomes injected mice was monitored by comparing the results of Western blots of tissues of wild type mice with or without administration of RLIP76 proteoliposomes.

Hyperinsulinemic-euglycemic and hyperglycemic clamp experiments*:* Hyperinsulinemic-euglycemic and hyperglycemic clamp experiments were performed by the Mouse Metabolic Phenotyping Center at the Yale University, School of Medicine, with procedures approved by Yale University IACUC. Briefly, $RLIP76^{+/+}$ and $RLIP76^{-/-}$ mice were anesthetized with an intraperitoneal injection of ketamine and xylazine, and a catheter was inserted in the right jugular vein and a 3-way connector was attached to the jugular vein catheter for intravenous infusion, and the blood samples were obtained from the tail vessels requiring a small tail cut. A 2-hour hyperinsulinemic-euglycemic clamp was conducted with a primed-continuous infusion of human insulin at a rate of 15 pmol/kg/min to raise plasma insulin within a physiological range (~300 pM). Blood samples were collected at 10-20 min intervals for the immediate measurement of plasma glucose concentration, and 20% glucose was infused at variable rates to maintain glucose at basal concentrations (~6 mM). Insulin-stimulated whole body glucose metabolism was assessed with a continuous infusion of 3-[^{3}H] glucose (0.1mCi /min) throughout the clamps. Basal rates of whole body glucose turnover were assessed using a primed-continuous infusion of 3-[^{3}H] glucose for 2 h prior to the start of clamp. To estimate insulin-stimulated glucose uptake in individual tissues, 2-deoxy-D-1-[^{14}C] glucose (2-[^{14}C] DG) is administered as a bolus (10 mCi) at 75 min after the start of clamp. Blood samples were taken at 0-120 min of clamp for the measurement of plasma 3-[^{3}H] glucose, and/or 2-[^{14}C] DG concentrations. Additional blood samples were collected before and at the end of clamp for the measurement of plasma insulin concentrations. A 2-hour hyperglycemic clamp is conducted with a variable infusion of 20% glucose to raise and maintain plasma glucose concentrations at ~16 mM. Blood samples were collected at 10-20 min intervals for the immediate measurement of plasma glucose concentrations using Beckman Glucose Analyzer. The area under curve of plasma glucose and insulin profiles was assessed to determine glucose-induced insulin secretion *in-vivo* (28).

Phosphoenolpyruvate carboxykinase (PEP-CK) Fructose 1, 6-bisphosphatase (F-1, 6-BPase) and glucose-6-phosphatase (G-6-Pase) activity in wild type and RLIP76 knockout mouse: The method of Opie and Newsholme (29) was used for PEP-CK assay.

F-1, 6-BPase was assayed by the method of Taketa and Pogell (30). G-6-Pase activity was determined using the method of Gierow and Jergil (31). Expression of PEP-CK, F-1,6 BPase, and G-6-Pase genes in wild-type ($RLIP76^{+/+}$) and RLIP76 knockout ($RLIP76^{-/-}$) mouse liver tissues was also quantitated by RT-PCR analysis using Qiagen RT-PCR kit following manufactures instructions. Briefly, liver tissues were placed in RNA-later reagent and RNA was isolated using RNeasy tissue kit (Qiagen) and was quantified and purity was determined by measuring absorbance at 260 and 280 nm. All primers were designed to have a T_m of 60 $\pm$ 5 ^oC. Gene specific primers [PEPCK: upstream primer 5' GAGTATATCCACATCT GCGATGGC and reverse primer was 5' GGCGAGTCTGTCAGTTCAATACCAATC, yielding 400 bp product; F-1,6 BPase: upstream primer 5'GCTCAACTCGATGCTGACTGCC and reverse primer 5' ACCAGGGTTCGACTACCATACAGTG, yielding 350 bp product; and for G-6-Pase: upstream primer 5'AGCTGTGGGCATTAAACTCC and downstream primer 5' AATGCCTGACAGGACTCCAG, yielding the product of 400 bp], were used for RT-PCR. The RT-PCR product was run on 1% agarose gel and bands were quantified using Alpha Imager HP. The ß-actin was used as an internal control.

FITC-conjugated insulin binding and internalization assay: RLIP76 MEFs (0.1 x 10^6 cells/ml) were grown on sterilized glass cover slips (18 mm size) in RPMI-1640 medium in tissue culture treated 12 well plates for overnight, followed by washing with PBS. Cells were incubated with 100 ng/ml FITC-conjugated insulin (prepared in PBS containing 1% BSA) for 60 min in ice (4 ^oC). Cells were then incubated at 37 ^oC in humidified chamber for 10 min followed by fixation with 4% paraformaldehyde. Slides were analyzed using confocal laser scanning microscopy with Zeiss 510-meta system, with excitation at 555 nm and emission 580 nm.

Preparation and application of insulin-QD: Insulin-QD complexes were formed by incubation of insulin (100 nM, from Gibco BRL) with QDs 605 ITK (from Molecular Probes) at 4 °C with mixing for 30 min. A molar ratio of 6:1 of insulin: QDs was used. To remove unbound ligand, the complexes were purified by chromatography over P30 size-exclusion spin columns (Bio-Rad, CA).

Transfection of $RLIP76^{-/-}$ MEFs with RLIP76-pEGFP-C1 vector and Insulin-QD labeling: $RLIP76^{-/-}$ MEFs were transiently transfected with pEGFP-C1 vector alone or with RLIP76-pEGFP-C1 vector using Lipofectamine 2000 (Invitrogen, Carlsbad, CA). $RLIP76^{-/-}$ control and $RLIP76^{-/-}$ transfected MEFs (0.1 x 10^6) were grown on sterilized glass cover slips in RPMI-1640 medium in tissue culture treated 12 well plates overnight. Cells were labeled with insulin:QD for 45 min at 4 ^oC, washed with PBS, incubated for 10 min at 37 °C, and fixed in 4% paraformaldehyde. Slides were analyzed by confocal laser scanning microscopy with Zeiss 510 meta system (ex 594 / em 610 for insulin:QD and ex 488 / em 507 nm for GFP-RLIP76).

FRET analysis: $RLIP76^{-/-}$ MEFs were transiently transfected with pEGFP-C1 vector alone or with RLIP76-pEGFP-C1 vector using Lipofectamine 2000 (Invitrogen, Carlsbad, CA). Transfection-efficiency was measured by fluorescent microscope (ex / em 488 / 507 nm), and RLIP76 mRNA expression was evaluated by RT-PCR analysis. $RLIP76^{-/-}$ control and $RLIP76^{-/-}$ transfected MEFs (1 x 10^5) were grown on sterilized glass cover slips in RPMI-1640 medium in 12 well plates for overnight and were treated with 10 µM doxorubicin or 10 µM glutathione-mono-chlorobimane for 20 min at 37 ^oC, washed with PBS and fixed in 4% paraformaldehyde. Molecular

interactions were visualized by FRET as described (32).

Statistical Methods: All data were evaluated with a two-tailed unpaired student's t test or compared by one-way ANOVA and are expressed as the mean $\pm$ SD. A value of $P < 0.05$ was considered statistically significant.

RESULTS

RLIP76 Gene Interruption Causes Hypoglycemia and Apparent Insulin Sensitivity: The baseline blood-glucose (BG) in $RLIP76^{-/-}$ mice was 46 % lower than in $RLIP76^{+/+}$ animals ($p<0.001$). At 2 h post insulin, BG dropped by 55 % in $RLIP76^{+/+}$ vs. 67 % in $RLIP76^{-/-}$ ($p<0.01$) (Fig. 1A). At 24 post-insulin (Fig 1B), BG levels had returned to baseline in all animals. The $RLIP76^{+/+}$ had quantitatively a very similar response to re-administration of insulin on day 2. However, the insulin sensitivity was magnified in $RLIP76^{-/-}$ mice, all of whom died of profound hypoglycemia within 90 min of insulin injection on the second day (Fig. 1C). These remarkable results indicated that $RLIP76^{-/-}$ mice are more insulin sensitive, and suggested that RLIP76 could function to antagonize insulin.

RLIP76 Gene Interruption Improves Glucose Tolerance and Plasma Lipid Levels: Additional evidence for insulin-sensitivity was sought in studies of glucose tolerance. BG levels after oral challenge of 2g/Kg.B.W. glucose were consistently and significantly lower in the $RLIP76^{-/-}$ as compared with wild-type (Fig. 2A) ($p<0.001$). In the non-fasting state, blood-glucose in $RLIP76^{-/-}$ mice was 46% lower in this study (Fig. 2B), consistent with results above (Fig. 1). Fasting BG in the $RLIP76^{-/-}$ mice decreased by <10%, whereas in the $RLIP76^{+/+}$ mice had a 35% reduction upon fasting. In addition, $RLIP76^{-/-}$ mice had lower total serum cholesterol and triglycerides (43% and 40% of control, respectively; $p< 0.01$) (Fig. 2C & D). The hypoglycemia is particularly remarkable because oxidative-stress (levels of lipid-hydroperoxides, lipid-alkenals, and alkenal-glutathione conjugates) is remarkably increased in the tissues of the $RLIP76^{-/-}$ animals (23, 27, 33, 34). This observation implies that in the absence of RLIP76, increases in these lipid-peroxidation products are insufficient by themselves to turn on any signaling pathway that can increase BG or lipids.

RLIP76 protein level correlates with insulin-glucose ratio: The ratio of insulin to BG (a measure of insulin-resistance) was lower in $RLIP76^{+/-}$ or $RLIP76^{-/-}$ mice as compared with $RLIP76^{+/+}$ animals ($p < 0.001$) (Fig. 3A). Insulin levels in all females were lower, and less affected by the loss of RLIP76 (Fig. 3B). Insulin-sensitivity appeared to increase with loss of RLIP76, predicted that increasing tissue RLIP76 should increase insulin-resistance. We examined the effect of augmenting RLIP76 in $RLIP76^{+/+}$ animals using i.p. injection of purified recombinant human RLIP76 protein encapsulated in liposomes (Fig. 3). Previous studies have defined the purity, stability, and tissue-pharmacology for RLIP76 delivery by these liposomes (22, 27, 35, 36). BG measurements were performed 24 h after i.p. injection of liposomes prepared with or without RLIP76 protein. Western blots of tissue homogenates and specific ELISA assays showed significantly augmented RLIP76 in mouse tissues at 24 h after i.p. injection (Fig. 3A&B, insets). The insulin/glucose ratio was increased in a stepwise fashion with respect to RLIP76 dose, also more prominently in males than females. Greater insulin-sensitivity of knockout mice was confirmed by QUICKI (37) as well as HOMA (38) analyses for insulin-resistance as well. These findings indicated that increased tissue RLIP76 increases insulin-resistance.

Hyperinsulinemic-euglycemic and hyperglycemic clamp studies demonstrate peripheral and hepatic insulin-sensitivity of

RLIP76$^{-/-}$ mice: Glucose homeostasis was compared in RLIP76$^{+/+}$ vs. RLIP76$^{-/-}$ mice using hyperinsulinemic-euglycemic and hyperglycemic clamp. The RLIP76$^{-/-}$ mice were smaller and had lower fat and muscle mass. Glucose clamp was successful in maintaining stable BG during the 140 min study (Fig. 4A). The glucose infusion rate required to maintain the same glucose level was almost two-fold greater in the RLIP76$^{-/-}$ mice (Fig. 4B). The whole body insulin sensitivity index, total peripheral-glucose uptake, hepatic glycolysis, glycogen synthesis, and hepatic insulin sensitivity index in the basal state were also greater in the RLIP76$^{-/-}$ mice (Fig. 4C). Under glucose clamp conditions, hepatic glucose output was markedly reduced in the RLIP76$^{-/-}$ animals (Fig. 4D). The remarkable difference indicates that RLIP76 functions to inhibit the turning off of gluconeogenesis during the fed-state. Since RLIP76 is a stress-inducible protein, these findings strongly indicate that conditions of stress that may increase hepatic RLIP76 levels would tend to antagonize the normal decrease in hepatic gluconeogenesis in the fed-state, potentially exacerbating stress hyperglycemia.

Cortisol induced hyperglycemic response is intact in RLIP76$^{-/-}$ animals: The above observations led to the obvious question of how RLIP76 interacts with cortisol, the most important stress-protective hormone, as well as the hepatic enzymes that regulate gluconeogenesis, phosphoenolpyruvate kinase (PEP-CK) and fructose-1,6-bisphosphatase (F-1,6-BP). Cortisol induced hyperglycemia was preserved in RLIP76$^{-/-}$ animals, who had a similar degree of cortisol induced rise in BG as in RLIP76$^{+/+}$ (Fig. 5).

RLIP76$^{-/-}$ mice have lower activity of PEP-CK, F-1,6-BPase and G6Pase: Though RLIP76 and cortisol effects on BG appeared independent, it was clear that the absolute BG in cortisol treated RLIP76$^{+/+}$ animals was greater than could be achieved in RLIP76$^{-/-}$ animals. We reasoned that this could be due to effects of RLIP76 loss on the three principal enzymes that regulate hepatic gluconeogenesis, PEP-CK, F-1,6-BPase, and G6Pase. To address this possibility, we compared the mRNA levels and activity of these enzymes between RLIP76$^{+/+}$ and RLIP76$^{-/-}$ mouse liver tissue. There was no difference in expression of PEP-CK, F-1,6-BPase, or G6Pase mRNA (Fig. 6A); despite this, the specific activity of all three proteins was substantially lower in the RLIP76$^{-/-}$ mouse liver. Comparison of these activities in RLIP76$^{+/+}$ vs. RLIP76$^{-/-}$ mouse liver homogenate treated without or with overnight dialysis showed that dialyzable inhibitors were present, but could not account for the lower activity of these enzymes in RLIP76$^{-/-}$. 4-HNE, an alkenal shown to increase 2-3 fold in RLIP76$^{-/-}$ mouse liver (33, 34), did not directly affect the activity of PEP-CK or G6Pase, but activated F-1,6-BPase activity. It is remarkable that despite decreased activity of these key gluconeogenic enzymes, hepatic glucose output was clearly increased in the knockout animals (Fig. 6B-E).

Baseline and oxidative-stress-induced insulin-endocytosis is deficient in RLIP76$^{-/-}$ MEFs: Our previous studies in MEFs derived from RLIP76$^{-/-}$ and RLIP76$^{+/+}$ mice have shown that clathrin-dependent endocytosis of EGF-receptor is markedly decreased in RLIP76$^{-/-}$ MEFs. Since clathrin-dependent endocytosis has been shown to be a primary mechanism for uptake of the insulin/insulin-receptor complex (thus terminating, or antagonizing, insulin signaling), we compared the uptake of fluorescein-labeled insulin between RLIP76$^{+/+}$ vs. RLIP76$^{-/-}$ MEFs. Results of these studies confirmed that insulin-endocytosis is clearly deficient in RLIP76$^{-/-}$ MEFs (Fig 7A). Oxidative stress in the form of hydrogen peroxide exposure caused a marked increase in endocytosis of quantum-dot labeled insulin-rhodamine in the RLIP76$^{+/+}$ MEFs, whereas this stress-

mediated effect was absent in RLIP76$^{-/-}$ MEFs (Fig. 7B). Taken together, these results offer strong support for a model in which RLIP76 functions to antagonize insulin-signaling, and that stress-conditions known to induce RLIP76 would tend to exacerbate insulin-resistance (20, 26, 39).

Analysis of interactions between RLIP76, its transported substrates, and insulin by FRET: To directly determine whether RLIP76 migrated with insulin in the endocytic vesicle, we expressed GFP-RLIP76 into RLIP76$^{-/-}$ MEFs, and examined the endocytosis of rhodamine-labeled insulin using confocal laser microscopy and FRET analysis (Fig. 7C). These studies also demonstrated that in the internalization of rhodamine-labeled insulin was also deficient in RLIP76$^{-/-}$ MEFs. Whereas empty GFP vector protein did not affect the internalization of rhodamine-insulin, transfection of RLIP76-GFP restored the internalization of insulin.

Since insulin is present on the outside of the cell membrane, and RLIP76 is associated with the endocytosis machinery on the inner membrane leaflet, we predicted that though the red and green fluorescence is internalized together, that there should be no direct FRET interaction between the red and green because the distance between the two fluorescent ligands should exceed 100 nm. Results of FRET analysis were consistent with this prediction (Fig. 7D).

FRET analysis can demonstrate specific binding of transported substrates to RLIP76 : The validity of the FRET analysis was confirmed using the fluorescent anthracycline drug, doxorubicin, which is known to bind to RLIP76 as well as GSH-monochlorobimane. Results of FRET studies are presented in Figure 8. The top images show the observed intensities for respective samples and below the histogram graph presents observed fluorescence lifetime measured for the respective images (Figs. 8A & B). For mono-chlorobimane (MCB) alone (histogram in red), the signal is very bright and the fluorescence lifetime is long, as expected about 9 ns with the relatively narrow distribution (Fig. 8B). Addition of RLIP76-GFP results in dramatic shortening of MCB fluorescence lifetime that drops to about 4 ns (histogram in red). The lifetime distribution is now relatively broad. This could reflect small heterogeneity of distances and/or relative orientations between MCB chromophore and GFP. Such shortening of donor fluorescence lifetime indicates strong interaction (very close proximity of two molecules) what is entirely consistent with our hypothesis. The right lower panel (Fig. 8C) shows the lifetime histogram for GFP only (green) and fluorescence of GFP in the presence of DOX (blue). The fluorescence lifetime of GFP in the presence of DOX is shorter confirming that DOX did clearly interact with the green fluorescence protein of RLIP76. The interaction of GSH-monochlorobimane fluorescent conjugate was much more clearly evident and indicated specific binding of the conjugate (Fig. 8B).

Effect of RLIP76 loss or augmentation on basal and insulin-stimulated change in glucose uptake and RTK-signaling: RLIP76$^{+/+}$ and RLIP76$^{-/-}$ MEFs were transfected with pcDNA3.1 empty vector (V) or pcDNA3.1 with full-length RLIP76 cDNA (R) using Lipofectamine (Invitrogen). Western-blot analyses of the 28,000 x g crude supernatant of homogenate of these cells against anti-RLIP76 IgG to demonstrated the absence of RLIP76 antigen in RLIP76$^{-/-}$ MEFs, and to showed increased RLIP76 protein upon transfection in both RLIP76$^{+/+}$ an RLIP76$^{-/-}$ MEFs (Fig. 9, panel A). A factorial experiment (2 [genotype] x 2 [RLIP76 over-expression] x 2 [anti-RLIP76 antibody] x 2 [insulin]) was designed to measure and compare the effect of insulin on glucose uptake, Foxo-1 inactivation, and activation of Akt, JNK and Hsf-1. The

results, normalized to the control group, RLIP76$^{+/+}$ MEFs transfected with empty vector, treated with no insulin and pre-immune IgG are presented (Fig. 9, panels B-D). In control RLIP76$^{+/+}$ MEFs, treatment with anti-RLIP76 IgG, previously shown to inhibit the transport activity of RLIP76 by binding to a cell surface epitope, caused a significant increase in activation of Hsf-1, JNK and Akt, a slight suppression of Foxo, and a 40% increase in uptake of glucose, in the absence of insulin. This finding indicated that inhibition of RLIP76 in normal cells activates stress pathways, and increases uptake of glucose through an insulin-independent mechanism. Insulin caused the expected effects of >2-fold increase in glucose-uptake, accompanied by activation of Hsf-1, Akt and JNK, and inactivation of Foxo. In the presence of both insulin and anti-RLIP76 IgG, glucose-uptake as well as signaling changes were greater than with either agent alone, and the net effect was consistent with an additive effect.

RLIP76 over-expression in the RLIP76$^{+/+}$ MEFs caused an effect opposite to that of the antibody, a suppression of Hsf-1, JNK and Akt, and activation of Foxo, as well as a reduction of glucose-uptake to half that seen with empty-vector transfection. Treatment of RLIP76 over-expressing RLIP76$^{+/+}$ MEFs with antibody restored Hsf-1, Akt and JNK as well as glucose-uptake to slightly greater than control. Treatment with insulin resulted in expected increase in Hsf-1, Akt, JNK and decrease in Foxo, but the magnitude of this response was suppressed significantly. Most strikingly, the glucose-uptake in-response to insulin, though about 1.8 fold compared with the absence of insulin, was still less than the control, and only 1/3 of that seen in empty-vector transfected cells. As in the vector-transfected cells, anti-RLIP76 IgG pre-treatment resulted in augmentation of insulin response with respect to Hsf-1, JNK and Akt, but suppression of Foxo was less prominent as compared with control. These observations argue strongly for the assertion that RLIP76 functions to antagonize insulin-signaling broadly and directly, and that conditions in which RLIP76 is elevated result in decreased response to insulin (resistance). Furthermore, RLIP76 also functions to antagonize insulin-independent glucose uptake as might be expected if glucose transporters are also subjected to increased rate of endocytosis.

Consistent with this model, the comparison of RLIP76$^{+/+}$ MEFs with RLIP76$^{-/-}$ MEFs showed a higher baseline activation of Hsf-1, JNK and Akt, and lower Foxo. Glucose-uptake in the absence of insulin in the RLIP76$^{-/-}$ MEFs was 60% higher as well, indicating that the lack of RLIP76 results in a state in which basal (insulin-independent) uptake of glucose is increased. This is likely to be the major underlying explanation for the fasting hypoglycemia, and increased glucose utilization in the RLIP76$^{-/-}$ mice. As expected, anti-RLIP76 IgG treatment of RLIP76$^{-/-}$ MEFs did not cause a significant change in the parameters measured. Insulin responsiveness with respect to changes in Hsf-1, JNK, Akt and Foxo was preserved in RLIP76$^{-/-}$ cells, though the fold change in glucose-uptake was actually slightly lower. This was due to a higher baseline insulin-independent signaling effects and glucose-uptake, and a likely ceiling effect of maximal possible glucose uptake, possibly determined by the number of glucose transporters present for translocation to the membrane. The anti-RLIP76 IgG had no effect on these parameters in RLIP76$^{-/-}$ MEFs, indicating that observed effects of this antibody in RLIP76$^{+/+}$ MEFs is due to a specific interaction of these antibodies with RLIP76 rather than any non-specific effect.

Transfection of RLIP76 into RLIP76$^{-/-}$ MEFs resulted in restoration of the pattern of signaling and glucose-uptake rate to that found in control RLIP76$^{+/+}$ MEFs; after transfection with RLIP76, response to anti-

RLIP76 IgG (in terms of increased glucose-uptake and increased signaling) was restored. Though the magnitude of insulin-response was blunted somewhat as compared with the un-transfected RLIP76$^{-/-}$ MEFs, transfection with RLIP76 caused a heightened response when cells were treated with both insulin and anti-RLIP76 IgG.

Taken together, these findings are consistent with a model in which RLIP76 functions to antagonize peripheral cellular glucose-uptake through both insulin-dependent as well as insulin-independent mechanisms, and conditions that increased RLIP76 should result in reduced uptake of glucose in peripheral cells.

DISCUSSION

Our studies show that RLIP76 regulates blood glucose by controlling insulin-dependent and insulin-independent mechanisms of cellular glucose uptake in both peripheral and hepatic tissues. The striking lack of endocytosis in RLIP76$^{-/-}$ MEFs appears to be the major overall perturbation responsible for the observed global effects on glucose homeostasis and signaling. The central role of RLIP76 in glycemic regulation is also evident from paradoxical findings, of marked insulin-sensitivity despite the presence of several fold-increased levels of oxidative-stress-derived free-radicals, lipid-peroxidation products and activated JNK, and p38 (23-27, 33, 39). If small-molecule products of oxidative degradation could themselves increase insulin-resistance, we should expect that RLIP76$^{-/-}$ mice should be quite insulin resistant since they have several fold higher levels of tissue hydroperoxides as compared with RLIP76$^{+/+}$ mice (23, 33, 34); this was obviously not the case.

To explain this apparent paradox, our model proposes that lipid peroxidation products mediate insulin-resistance because their GS-E are necessary substrates for RLIP76 to drive the process of endocytosis – in the absence of RLIP76 and of endocytosis, the 'dwell-time' of insulin at the plasma membrane is greater, resulting in greater insulin sensitivity. Increasing RLIP76 in cells inhibits insulin-independent glucose uptake, and antagonizes insulin-independent glucose uptake. Because clathrin-dependent endocytosis exerts broad effects on receptor-ligand signaling (including G-protein-linked receptors) as well as on trafficking of membrane proteins (such as GLUT), the insulin-independent effects are understandable, and in some ways expected. Because lipid trafficking between peripheral and hepatic tissues is also intricately linked with clathrin-dependent endocytosis (23-25, 39), it is also perhaps not surprising that both blood cholesterol and triglycerides were lower in RLIP76$^{-/-}$ animals. These findings are of clinical interest, because both hyperglycemia and hyperlipidemia could be treated by targeting RLIP76. Because RLIP76 is a known stress-inducible protein conditions that increase RLIP76 expression (i.e. oxidative stress) will cause insulin-resistance and hyperlipidemia. More importantly, in the absence of RLIP76, oxidative stress alone is insufficient to mediate insulin-resistance (23, 26).

The central stress-response role of RLIP76 is also evident from the effects of RLIP76 loss on stress-responsive-kinase signaling, which are activated but insufficient to mediate insulin-resistance. Elevated heat-shock proteins are expected because RLIP76 is known to bind to and sequester Hsf-1, the master transcriptional regulator of the heat-shock response. Thus RLIP76 functions as the primary regulator (inhibitor) of transcription of chaperones, which are dramatically increased in tissue of RLIP76$^{-/-}$ mice (33, 36, 39). Decreased levels of chaperone heat-shock proteins have been correlated with insulin-resistance (40); thus elevated chaperone levels could also contribute to the observed insulin-sensitivity of RLIP76$^{-/-}$mice. MEF studies show that

Hsf-1, JNK and Akt are activated, and their activation is directly correlated with glucose uptake in response to insulin; FOXO is inactivated by insulin, and its activity is inversely correlated with insulin-dependent glucose uptake. All signaling responses are blunted by RLIP76 over-expression, again emphasizing the overarching role of clathrin-dependent endocytosis in signaling regulation, and the crucial rate-regulatory role of RLIP76 in clathrin-dependent endocytosis.

Increased insulin sensitivity in short-term (clamp-studies) in both peripheral and hepatic tissues of C57B mice, and the dramatic effects of repeat insulin administration in $RLIP76^{-/-}$ animals are entirely consistent with our model. In the absence of RLIP76, in the fed-state, hepatic glucose output is nearly abrogated in $RLIP76^{-/-}$ mouse, whereas it is only slightly suppressed in $RLIP76^{+/+}$; these finding imply that inhibition of RLIP76 could have a salutary effect by reducing hepatic glucose output. The complex interactions of insulin-dependent and insulin-independent regulators of glycemic control in the whole animal is likely to yield interesting and perhaps paradoxical observations with further experimental manipulations planned to evaluate the effects of RLIP76 loss on interactions between diet, insulin, glucagon, and glucocorticoids.

Gucocorticoid mediated hyperglycemia is known to be mediated both through increased gluconeogenesis (41) and through increased insulin-resistance (42). Diminished hyperglycemic effect of hydrocortisone in $RLIP76^{-/-}$ mice indicates a regulatory role of RLIP76 in glucocorticoid action. It should be noted that glucocorticoid receptor knockout mice are only hypoglycemic when stressed; $RLIP76^{-/-}$ mice are hypoglycemic at baseline – despite the fact that they have relatively higher hepatic glucose output than the $RLIP76^{+/+}$ mice. These observations imply a fundamental increase in both hepatic and peripheral insulin-sensitivity in $RLIP76^{-/-}$ mice.

Present studies have important implications in the understanding of mechanisms governing the phenomenon of insulin-resistance associated with clinical disease conditions in which oxidative stress is increased. They predict that an invariable consequence of oxidative stress is an increase in formation of GS-E in cells, resulting in an increased rate of their efflux, and a consequent increase in the rate of internalization of membrane receptor/ligand complexes; by the same token, conditions or agents which reduce oxidative stress and GS-E formation should result in an increased 'dwell-time' of receptor/ligand couples in plasma membrane, increasing signaling efficiency. Another important corollary to present findings is that small molecules that interact with RLIP76, either at the cell-surface or internally at one or more sites known to regulate its transport activity, could potentially function as novel hypoglycemic and hypolipidemicagents.

ACKNOWLEDGMENTS

This work was supported in part by NIH Grants CA 77495 and CA 104661 (to SA), ES 012171(to YCA), Cancer Research Foundation of North Texas (to SSS & SY), Institute for Cancer Research and the Joe & Jessie Crump Fund for Medical Education (to SSS). The authors thank Center for Commercialization of Fluorescence Technologies (CCFT) at the University of North Texas Health Science Center, Fort Worth, TX, for helping in confocal laser and FRET analyses. We also thank Abhijit Bugde and Dr. Kate Luby-Phelps from The Live Cell Imaging Core Facility at The University of Texas Southwestern Medical Center at Dallas for help in imaging using the Lecia TCS SP5 confocal microscope.

REFERENCES

1 Tirosh A, Potashnik R, Bashan N, Rudich A. Oxidative stress disrupts insulin-induced cellular redistribution of insulin receptor substrate-1 and phosphatidylinositol 3-kinase in 3T3-L1 adipocytes. A putative cellular mechanism for impaired protein kinase B activation and GLUT4 translocation. J Biol Chem 1999;274:10595-10602.

2 Awasthi S, Singhal SS, Srivastava SK, Zimniak P, Bajpai KK, Saxena M, et al. Adenosine triphosphate- dependent transport ofdoxorubicin, daunomycin, and vinblastine in human tissues by a mechanism distinct from the P-glycoprotein. J Clin Invest 1994;93:958-965.

3 Yung LM, Leung FP, Yao X, Chen ZY, Huang Y. Reactive oxygen species in vascular wall. Cardiovasc Hematol Disord Drug Targets 2006;6:1-19.

4 Seddon M, Looi YH, Shah AM. Oxidative stress and redox signalling in cardiac hypertrophy and heart failure. Heart 2007;93:903-907.

5 Ceriello A. Acute hyperglycaemia and oxidative stress generation. Diabet Med 1997; 3:S45-49.

6 Tirosh A, Rudich A, Potashnik R, Bashan N. Oxidative stress impairs insulin but not platelet-derived growth factor signaling in 3T3-L1 adipocytes. Biochem J 2001;355:757-763.

7 Evans JL, Goldfine ID, Maddux BA, Grodsky GM. Are oxidative stress-activated signaling pathways mediators of insulin resistance and beta-cell dysfunction? Diabetes 2003;52:1-8.

8 Talior I, Yarkoni M, Bashan N, Eldar-Finkelman H. Increased glucose uptake promotes oxidative stress and PKC-delta activation in adipocytes of obese, insulin-resistant mice. Am J Physiol Endocrinol Metab 2003;285:E295-302.

9 Tiedge M, Lortz S, Drinkgern J, Lenzen S. Relation between antioxidant enzyme gene expression and antioxidative defense status of insulin-producing cells. Diabetes 1997; 46: 1733-1742.

10 Maechler P, Jornot L, Wollheim CB. Hydrogen peroxide alters mitochondrial activation and insulin secretion in pancreatic beta cells. J Biol Chem 1999;274:27905-27913.

11 Sakai K, Matsumoto K, Nishikawa T, Suefuji M, Nakamaru K, Hirashima Y, et al. Mitochondrial reactive oxygen species reduce insulin secretion by pancreatic beta-cells. Biochem Biophys Res Commun 2003;300:216-222.

12 Paz K, Hemi R, LeRoith D, Karasik A, Elhanany E, Kanety H, et al. A molecular basis for insulin resistance. Elevated serine/threonine phosphorylation of IRS-1and IRS-2 inhibits their binding to the juxtamembrane region of the insulin receptor and impairs their ability to undergo insulin-induced tyrosine phosphorylation. J Biol Chem 1997;272: 29911-29918.

13 Evans JL, Maddux BA, Goldfine ID. The molecular basis for oxidative stress-induced insulin resistance. Antioxid Redox Signal 2005;7:1040-1052.

14 Pessler D, Rudich A, Bashan N. Oxidative stress impairs nuclear proteins binding to the insulin responsive element in the GLUT4 promoter. Diabetologia 2001;44:2156-2164.

15 Frey RS, Gao X, Javaid K, Siddiqui SS, Rahman A, Malik AB. Phosphatidylinositol 3-kinase gamma signaling through protein kinase Czeta induces NADPH oxidase-mediated oxidant generation and NF-kappaB activation in endothelial cells. J Biol Chem 2006;281: 16128-16138.

16 Liochev SI, Fridovich I. How does superoxide dismutase protect against tumor necrosis factor: a hypothesis informed by effect of superoxide on "free" iron. How does superoxide dismutase protect against tumor necrosis factor: a hypothesis informed by effect of superoxide on "free" iron. Free Radic Biol Med 1997;23:668-671.

17 Esterbauer H, Schaur RJ, Zollner H. Chemistry and biochemistry of 4-hydroxynonenal, malonaldehyde and related aldehydes. Free Radic Biol Med 1991;11:81-128.

18 Awasthi YC, Yang Y, Tiwari NK, Patrick B, Sharma A, Li J, et al. Regulation of 4-hydroxynonenal-mediated signaling by glutathione S-transferases. Free Radic Biol Med 2004;37:607-619.

19 Feng Z, Hu W, Tang MS. Trans-4-hydroxy-2-nonenal inhibits nucleotide excision repair in human cells: a possible mechanism for lipid peroxidation-induced carcinogenesis. Proc Natl Acad Sci U S A. 2004;101:8598-8602.

20 Cheng JZ, Sharma R, Yang Y, Singhal, SS, Sharma A, Saini MK, et al. Accelerated metabolism and exclusion of 4-hydroxynonenal through induction of RLIP76 and hGST5.8 is an early adaptive response of cells to heat and oxidative stress. J Biol Chem 2001;276:41213-41223.

21 Singhal SS, Sehrawat A, Metha A, Sahu M, Awasthi S. Functional reconstitution of RLIP76 catalyzing ATP-dependent transport of glutathione-conjugate. Int J Oncol 2009;34:191-199.

22 Awasthi S, Cheng J, Singhal SS, Saini MK, Pandya U, Pikula S, et al. Novel function of human RLIP76: ATP-dependent transport of glutathione conjugates and doxorubicin. Biochemistry 2000;39:9327-9334.

23 Awasthi S, Singhal SS, Sharma R, Zimniak P, Awasthi YC. Transport of glutathione conjugates and chemotherapeutic drugs by RLIP76 (RALBP1): a novel link between G-protein and tyrosine kinase signaling and drug resistance. Int J Cancer 2003;106:635-646.

24 Rosse C, L'Hoste S, Offner N, Picard A, Camonis JH. RLIP76, an effector of the Ral GTPases, is a platform for Cdk1 to phosphorylate epsin during the switch off of endocytosis in mitosis. J Biol Chem 2003;278:30597-30604.

25 Singhal SS, Yadav S, Roth C, Singhal J. RLIP76: A novel glutathione-conjugate and multi-drug ransporter. Biochem Pharmacol 2009;77:761-769.

26 Singhal SS, Yadav S, Singhal J, Sahu M, Sehrawat A, Awasthi S. Diminished drug transport and augmented radiation sensitivity caused by loss of RLIP76. FEBS Lett 2008; 582:3408-3414.

27 Awasthi S, Singhal SS, Yadav S, Singhal J, Drake K, Nadkar A, et al. RLIP76 is a major determinant of radiation sensitivity. Cancer Res 2005;65:6022-6028.

28 Kim JK, Fillmore JJ, Sunshine MJ, Albrecht B, Higashimori T, Kim DW, et al. PKC-theta knockout mice are protected from fat-induced insulin resistance. J Clin Invest 2004; 114:823-827.

29 Opie LH, Newsholme EA. The inhibition of skeletal-muscle fructose 1,6-diphosphatase by adenosine monophosphate. Biochem J 1967;104:353-360.

30 Taketa K, Pogell BM. Allosteric inhibition of rat liver fructose 1,6-diphosphatase by adenosine 5'-monophosphate. J Biol Chem 1965;240:651-662.

31 Gierow P, Jergil,B. A spectrophotometric method for the determination of glucose-6-phosphatase activity. Anal Biochem 1980;101:305-309.

32 Gryczynski Z, Gryczynski I, Lakowicz. JR. Mol.Imag. FRET Microscopy and Spectroscopy. Oxford Unversity Press. A. Periasami and R. N. Day Eds. 2005, p. 21-56.

33 Singhal J, Singhal SS, Yadav S., Warnke M, Yacoub A, Dent P, et al. RLIP76 in defense of radiation poisoning. Int J Rad Oncol Biol Phys 2008;72:553-561.
34 Warnke MM, Wanigasekara E, Singhal SS, Singhal J, Awasthi S, Armstrong DW. The determination of glutathione-4-hydroxynonenal (GS-HNE), E-4-hydroxynonenal (HNE), and E-1-hydroxynon-2-en-4-one (HNO) in mouse liver tissue by LC-ESI-MS. Analyt Bioanalyt Chem 2008;392:1325-1333.
35 Rosse C, Hatzoglou A, Parrini MC, White MA, Chavrier P, Camonis J. RalB mobilizes the exocyst to drive cell migration. Mol Cell Biol 2006;26:727-734.
36 Singhal SS, Yadav S, Drake K, Singhal J, Awasthi S. Hsf-1 and POB1 induce drug sensitivity and apoptosis by inhibiting Ralbp1. Hsf-1 and POB1 induce drug sensitivity and apoptosis by inhibiting Ralbp1. J Biol Chem 2008;283:19714-19729.
37 Katz A, Nambi SS, Mather K, Baron AD, Follmann DA, Sullivan G, et al. Quantitative insulin sensitivity check index: a simple, accurate method for assessing insulin sensitivity in humans. J Clin Endocrinol Metab 2000;85:2402-2410.
38 Matthews DR, Hosker JP, Rudenski AS, Naylor BA, Treacher DF, Turner RC. Homeostasis model assessment: insulin resistance and beta-cell function from fasting plasma glucose and insulin concentrations in man. Diabetologia 1985;28:412-419.
39 Singhal SS, Awasthi S. Glutathione-conjugate transport and stress-response signaling: Role of RLIP76. In: Toxicology of Glutathione S-Transferases. (Y.C. Awasthi, Ed). CRC Press, Boca Raton, FL pp. 231-256, 2006
40 Kurucz I, Morva A, Vaag A, Eriksson KF, Huang X, Groop L, et al. Decreased expression of heat shock protein 72 in skeletal muscle of patients with type 2 diabetes correlates with insulin resistance. Diabetes 2002;51:1102-1109.
41 Yamashita R, Kikuchi T, Mori Y, Aoki K, Kaburagi Y, Yasuda K, et al. Aldosterone stimulates gene expression of hepatic gluconeogenic enzymes through the glucocorticoid receptor in a manner independent of the protein kinase B cascade. Endocr J 2004;51:243-251.
42 Andrews RC, Walker BR. Glucocorticoids and insulin resistance: old hormones, new targets. Clin Sci (Lond) 1999;96:513-523.

Figure Legends

Figure 1 Effect of intraperitoneal administration of insulin on blood sugar between RLIP76$^{+/+}$ and RLIP76$^{-/-}$ animals Level of BG at 2 h post insulin (**Panel A**) and at 24 h post-insulin (**Panel B**) after a single dose of insulin administered intraperitoneally. Re-administration of insulin on day 2, the RLIP76$^{+/+}$ BG level goes down. The insulin sensitivity of RLIP76$^{-/-}$ was magnified significantly, with death of all animals before 90 min (**Panel C**). BG at the time of death was undetectable. Symbols are as follows: RLIP76$^{+/+}$ (circles); RLIP76$^{-/-}$ (diamonds); Pink and blue colors indicate no insulin, and red and purple colors indicate insulin dosing.

Figure 2 Glucose tolerance test (GTT) and lipid levels in RLIP76$^{-/-}$ mice For the glucose-tolerance test, C57B mice (wild-type and RLIP76$^{-/-}$) were fasted for 6 h followed by oral administration of 2 g/Kg B.W. glucose using a gavage needle. Each of 5 groups consisted of 5 animals each. One group was sacrificed at each time point (0, 5, 30, 60, and 120 min) and ~ 200

– 300 µl of blood was sampled for glucose analyses. Blood was kept refrigerated for ~ 4 h, centrifuged at 3000 x g for 10 min, and the serum was separated and stored at- 20 ^{o}C until assay. Glucose, cholesterol and triglycerides measurement were performed in the laboratory of Dr. Kent R. Refsal, Michigan State University, Michigan. * Statistical analyses by ANOVA were significant at $p < 0.001$ for RLIP76$^{-/-}$ *vs.* RLIP76$^{+/+}$ animals, n = 5.

Figure 3 Insulin/glucose ratio in RLIP76 deficient and supplemented mice Twelve weeks old C57BL/6 mice born of heterozygous x heterozygous mating were genotyped by PCR. Insulin and glucose measurement in blood serum were performed on wild type (RLIP76$^{+/+}$) animals sacrificed 24 h after a single i.p. injection of control or RLIP76-liposomes equivalent to 200 and 500 µg RLIP76 protein. Insulin and glucose measurement in blood serum were also performed on heterozygous (RLIP76$^{+/-}$) and homozygous (RLIP76$^{-/-}$) animals. The values are presented as mean $\pm$ SD from three separate determinations with three replicates (n = 9) (**panels A and B**). Western-blot analyses for RLIP76 were performed on liver and heart tissues of RLIP76$^{+/+}$ male and female mice sacrificed 24 h after administration of 200 or 500 µg RLIP76 protein in the form of liposomes, i.p. Aliquots of 100 µg detergent solubilized crude membrane fraction from the liver and heart of animals treated with 200 µg (R2) or 500 µg (R5) were loaded per lane in SDS-PAGE, transblotted, and probed using anti-RLIP76 IgG primary and peroxidase-conjugated goat-anti-rabbit IgG secondary antibody. The blots were developed with 4-chloro-1-napthol as chromogenic substrate (**panels A and B insets**). β-actin expression was used as loading control. Statistical analyses by ANOVA were significant at $p < 0.01$ for RLIP76$^{-/-}$ *vs.* RLIP76$^{+/-}$, RLIP76$^{-/-}$ *vs.* RLIP76$^{+/+}$, RLIP76$^{+/-}$ *vs.* RLIP76$^{+/+}$, and RLIP76$^{+/+}$ *vs.* RLIP76-proteoliposomes treated RLIP76$^{+/+}$.

Figure 4 Hyperinsulinemic-euglycemic and hyperglycemic clamp studies

Glucose and insulin-clamp studies were performed as described in *Experimental Methods* at the Mouse Metabolic Phenotyping Center at the Yale University, School of Medicine, with procedures approved by Yale University IACUC. Panels A & B demonstrate the result of hyperinsulinemic-euglycemic clamp study in which the BG of both wild-type (circle) and RLIP76$^{-/-}$ animals (diamond) were maintained approximately equal for the 140 min duration of the study (**panel A**); the rate of glucose infusion required to maintain equal BG (**panel B**) was significantly greater for the RLIP76$^{-/-}$ animals as compared with wild-type controls at all experimental time points. Calculated total body glucose turnover, glycolysis and hepatic glycogen synthesis (**panel C**) and hepatic glucose output in a basal ('fasting') as well as hyperglycemic clamp ('fed') state (**panel D**) are presented. RLIP76$^{+/+}$ mice, black bars; RLIP76$^{-/-}$ mice, gray bars. Statistical analyses by ANOVA were significant at $p < 0.05$ for RLIP76$^{+/+}$ *vs.* RLIP76$^{-/-}$, n = 8.

Figure 5 The effect of hydrocortisone on the BG level of RLIP76$^{+/+}$ and RLIP76$^{-/-}$ animals Wild type and RLIP76 knockout mice were treated with hydrocortisone (1g/kg b.w.) and the BG level was checked in the blood drown from the tail at different time points from 0 to 120 min. $p < 0.01$, when compared RLIP76$^{+/+}$ *vs.* RLIP76$^{-/-}$animals, n = 5.

Figure 6 The activity of gluconeogenesis enzymes The activity of PEP-CK (**panel B**), F-1, 6 BPase (**panel C**) and G-6-Pase (**panel D**) was measured in un-dialyzed and dialyzed liver homogenates of RLIP76$^{+/+}$ and RLIP76$^{-/-}$ animals. The effect of 4-HNE was also determined on

the activity for all the three important enzymes of gluconeogenesis (**panel E**). The enzyme PEP-CK, catalyze the conversion of phosphoenolpyruvate to Fructose1,6-biphosphate in a series of steps involving oxidation of NADH to NAD. In this assay, the loss of NADH was determined spectrophotometrically by measuring absorbance at 340 nm, based on the method of Opie and Newsholme (29). For F-1, 6-BPase activity, a spectrophotometric coupled enzyme assay was used by a method of Taketa and Pogell (30). F-1, 6-BPase activity was coupled with phosphoglucose isomerase and NADP dependent glucose 6-phosphate dehydrogenase, and NADPH formation was measured at 340 nm. G-6-Pase activity was determined spectrophotometrically using the method of Gierow and Jergil (31). The method is based on a coupled enzyme reaction in which glucose formed is reacted with glucose oxidase and peroxidase and the quinoneimine formed is a colored product and its formation can be followed spectrophotometrically at 510 nm. The expression of all the three enzymes was determined by RT-PCR. (**panel A**) using their gene specific primers. Either dialyzed or un-dialyzed, $p < 0.01$, when compared $RLIP76^{+/+}$ *vs.* $RLIP76^{-/-}$. $RLIP76^{+/+}$ or $RLIP76^{-/-}$, $p < 0.07$, when compared un-dialyzed *vs.* dialyzed. Mean $\pm$ SD for three separate experiments, each in triplicates, are shown ($n = 9$).

Figure 7 Effect of RLIP76 on insulin internalization Insulin binding and internalization was studied in RLIP76 $MEF^{+/+}$ and RLIP76 $MEF^{-/-}$ using FITC-insulin. Cells (0.1×10^6 cells/ml) grown on the sterilized cover slips were incubation with FITC-insulin (100 ng/ml) for 45 minutes in ice followed by incubation for 10 min at 37 ^oC. Cells were fixed and analyzed by confocal laser microscopy. Photographs taken at identical exposure at 400 x magnification are presented **(panel A)**. **Stress-mediated effect on insulin internalization** $RLIP76^{+/+}$ and $RLIP76^{-/-}$ MEFs (0.1×10^6 cells/ml) were grown on cover slips, followed by incubation with 50 μM H_2O_2 for 20 min at 37 ^oC, and allowed to recover for 2 h. Cells were treated with molar ratio 6:1 of insulin-rhodamine:QD on ice for 45 min, washed and incubated for 10 min at 37 °C and fixed in cold 4% paraformaldehyde. Slides were analyzed using confocal laser-scanning microscopy. Photographs taken at identical exposure at 400 x magnification are presented **(panel B)**; **Effect of RLIP76 on insulin internalization using Insulin-QD complexes** Insulin binding and internalization was studied in $MEF^{+/+}$, $MEF^{-/-}$, and $MEF^{-/-}$ transfected with empty GFP vector and RLIP76-GFP vector, using insulin:QD complexes. Insulin-QD complexes were formed by incubation of insulin (40 nM, from GIBCO BRL) with QDs 605 ITK amino (PEG) (from Molecular Probes) at 4 °C for 30 min. A molar ration of 6:1 of insulin: QDs was used. Cells grown on the sterilized cover slips were treated with insulin:QD complexes for 10 min at 37 ^oC. Cells were fixed and analyzed using confocal laser scanning microscopy with Zeiss 510-meta system, with excitation at 594 nm and emission 610 nm. Photographs taken at identical exposure at 400 x magnification are presented (**panel C**). The molecular interactions between the RLIP76 and insulin were checked by the **F**orster **R**esonance **E**nergy **T**ransfer (FRET) analysis as described in the method section. The FRET analysis clearly indicated that there is no direct interaction of RLIP76 and insulin (**panel D**).

Figure 8 Binding of GSH-mono-chlorobimane and DOX by FRET analysis

Binding of GSH-mono-chlorobimane (GSH-MCB) and DOX was studied in $MEF^{-/-}$ and $MEF^{-/-}$ transfected with RLIP76-GFP vector. Cells grown on the sterilized cover slips were treated with either 50 μM mono-chlorobimane or 10 μM DOX and incubated at 37 ^oC for 20 minutes. Cells were fixed with 4% paraformaldehyde and FRET and molecular interactions in

the cell were analyzed by using time-resolved confocal microscope MT 200 (from Picoquant GmbH) with pulsed diode laser excitations at 405 nm (for MCB donor) and 475 nm (for GFP donor). For MCB observation, 465 nm (10 nm bend with) interference filter crossed with 430 nm long path cut-off and for GFP observation 490-530 nm interference filter crossed with 500 nm long path filter was used. The top images show the observed intensities for respective samples (**panel A**). Below the histogram graph presents observed fluorescence lifetime measured for the respective images. For MCB alone (histogram in red) the signal is very bright and the fluorescence lifetime is long, as expected about 9 ns with the relatively narrow distribution. Addition of RLIP76-GFP results in dramatic shortening of MCB fluorescence lifetime that dropped to about 4 ns (histogram in red) (**panel B**). The validity of the FRET analysis was confirmed using the fluorescent anthracycline drug, DOX, which is known to bind to RLIP76. **Panel C** shows the lifetime histogram for GFP only (green) and fluorescence of GFP in the presence of doxorubicin (DOX; blue). The fluorescence lifetime of GFP in the presence of DOX is shorter confirming that DOX did clearly interact with the green fluorescence protein of RLIP76.

Figure 9 Regulation of Signaling via Hsf-1, Akt, JNK and FOXO-1 by RLIP76

$RLIP76^{+/+}$ and $RLIP76^{-/-}$ MEFs were subjected to transfection with pcDNA3.1 empty vector (V) or pcDNA3.1 with full-length RLIP76 cDNA (R) using Lipofectamine (Invitrogen). Western-blot analysis of the 28,000 x g crude supernatant of homogenate of these cells were subjected to Western-blot analysis against anti-RLIP76 IgG to demonstrate the absence of RLIP76 antigen in $RLIP76^{-/-}$ MEFs, and to show increased RLIP76 protein upon transfection in both $RLIP76^{+/+}$ an $RLIP76^{-/-}$ MEFs. β-actin was used as an internal control (panel A). The effect of RLIP76 over-expression, insulin or anti-RLIP76 antibody on $RLIP76^{+/+}$ and $RLIP76^{-/-}$ MEFs on signaling as well as glucose uptake was carried out at 37 ^{o}C with 5% CO_2 atmosphere. The cells were pre-treated with either polyclonal rabbit pre-immune IgG (C or PIS) or anti-human-RLIP76 IgG fractions (AR) (40 μg/ml final conc.) for 1 h. Buffer containing ^{14}C-glucose and either no insulin or 20 mU insulin was added to start the measurement of glucose uptake, and the measurement was terminated at 30 min by washing off the medium with ice-cold PBS, and solubilization of cells in counting cocktail. Glucose uptake was measured in 5 x 10^6 cells as described previously (36). In parallel experiments where ^{14}C glucose was omitted, measurements of phosphorylation of Akt, Hsf-1, JNK, and inactivation of Foxo1 were performed also at 30 min. Results of Western-blot analyses of Hsf-1 expression and phospho-Akt (ser-473, Upstate Cell Signaling, NY) are presented. β-actin expression was shown to confirm equal amount of protein was loaded in each sample (panel B). Results from all groups were analyzed with plots of glucose uptake vs. Hsf-1 expression and Akt activation as well as Foxo-1 inactivation and Jun N-terminal kinase (JNK) phosphorylation (measured by ELISA assay, Active Motif, CA) (panel C). Results of all five measurements normalized to the control group ($RLIP76^{+/+}$ MEFs transfected with empty vector, treated with no insulin and pre-immune IgG) are presented (panel D). Mean $\pm$ SD for two separate experiments, each in triplicates, are shown (n = 6) (33, 36).

Figure 1

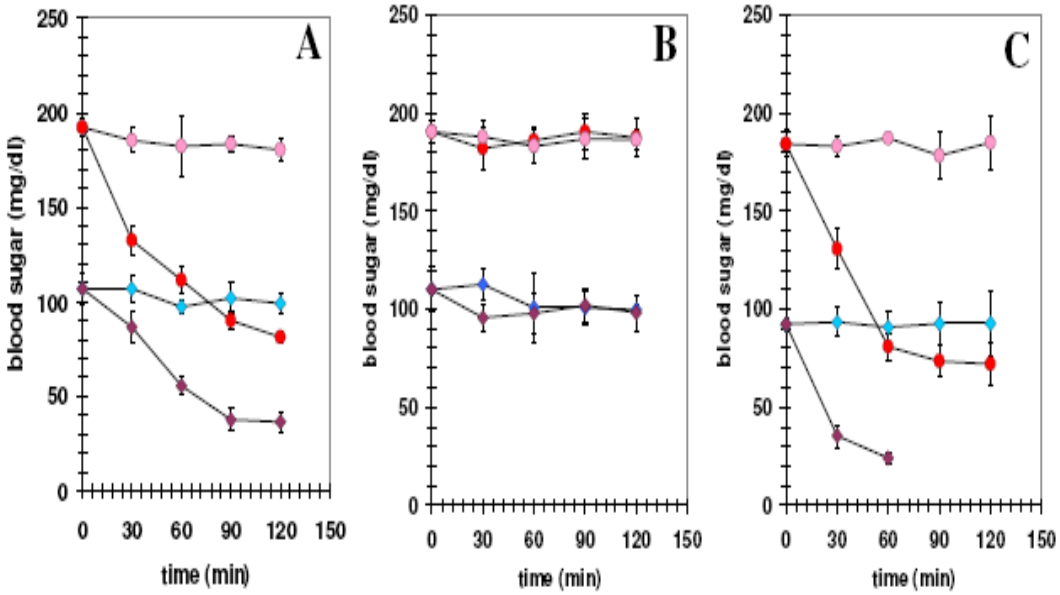

Figure 2

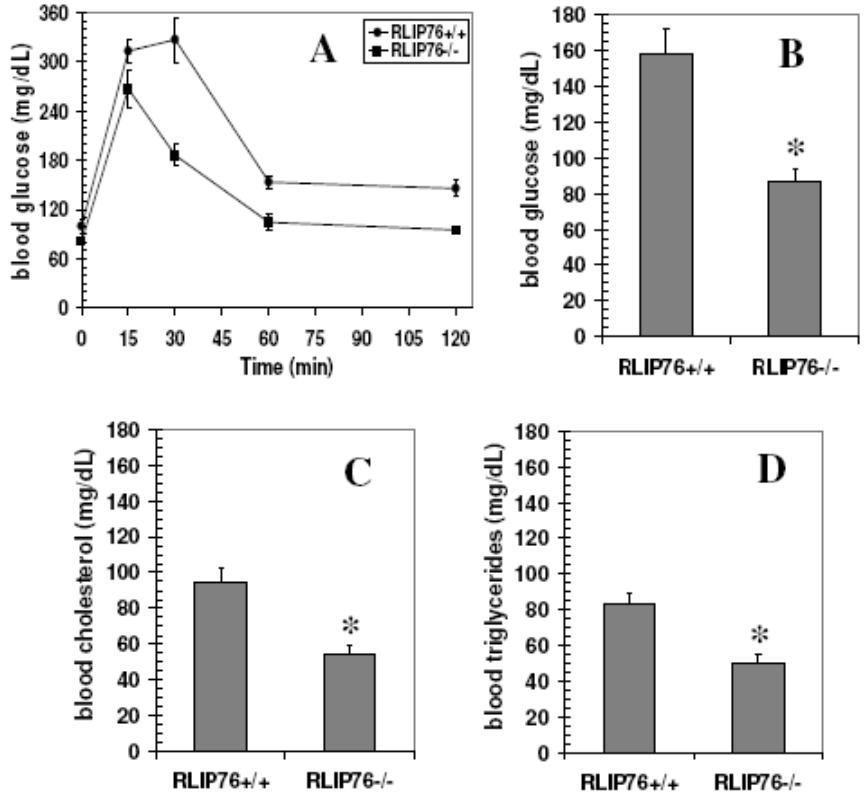

Figure 3

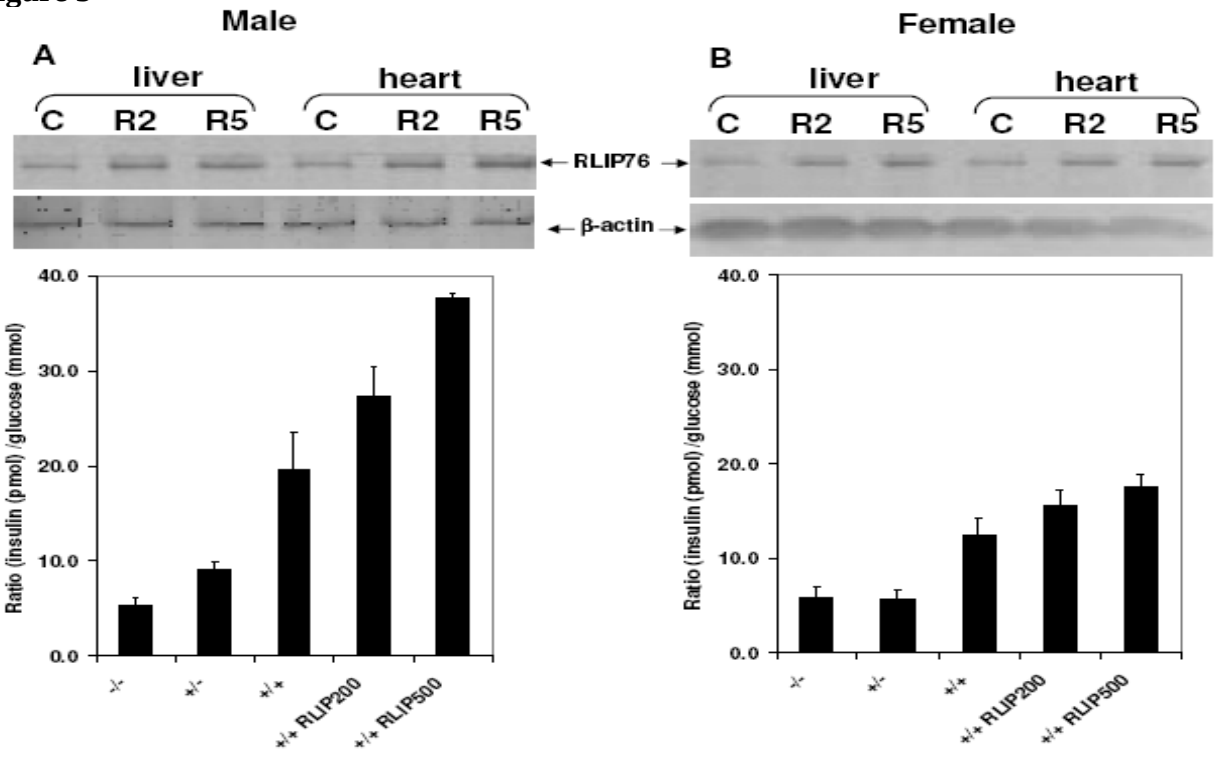

Figure 4

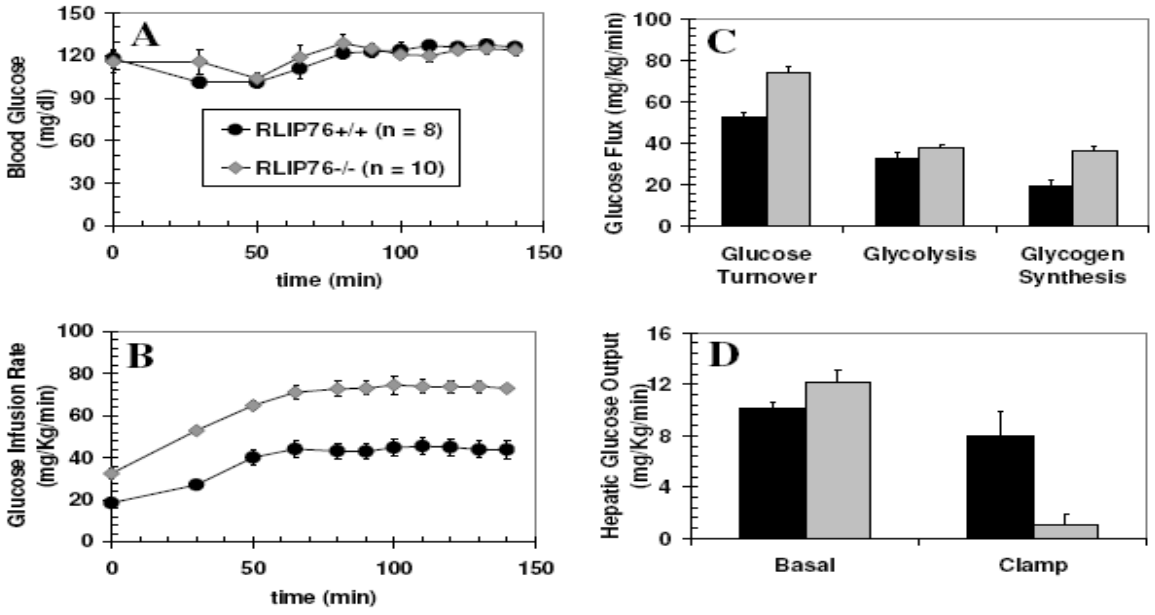

Figure 5

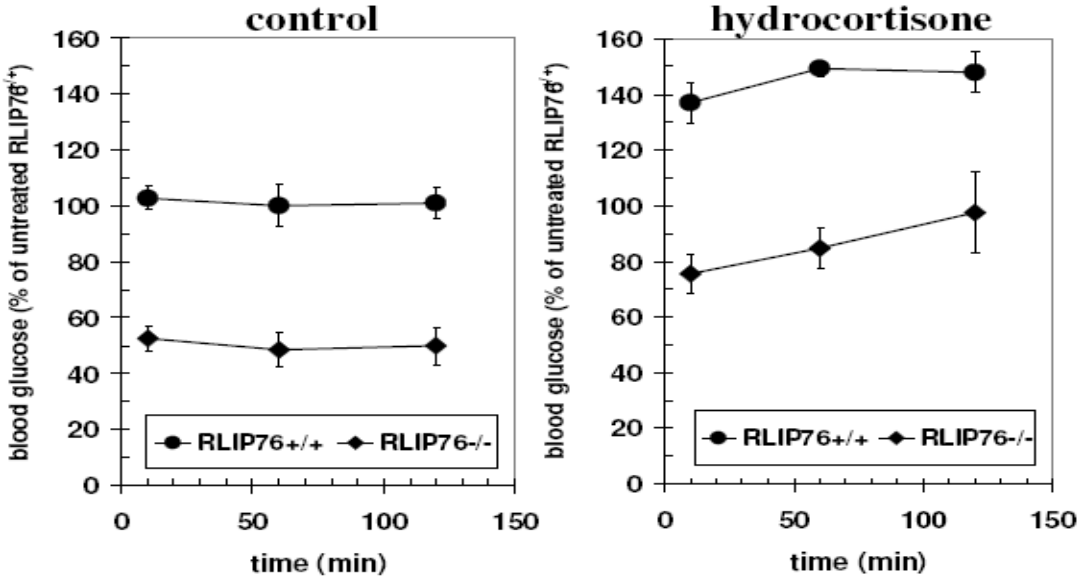

Figure 6

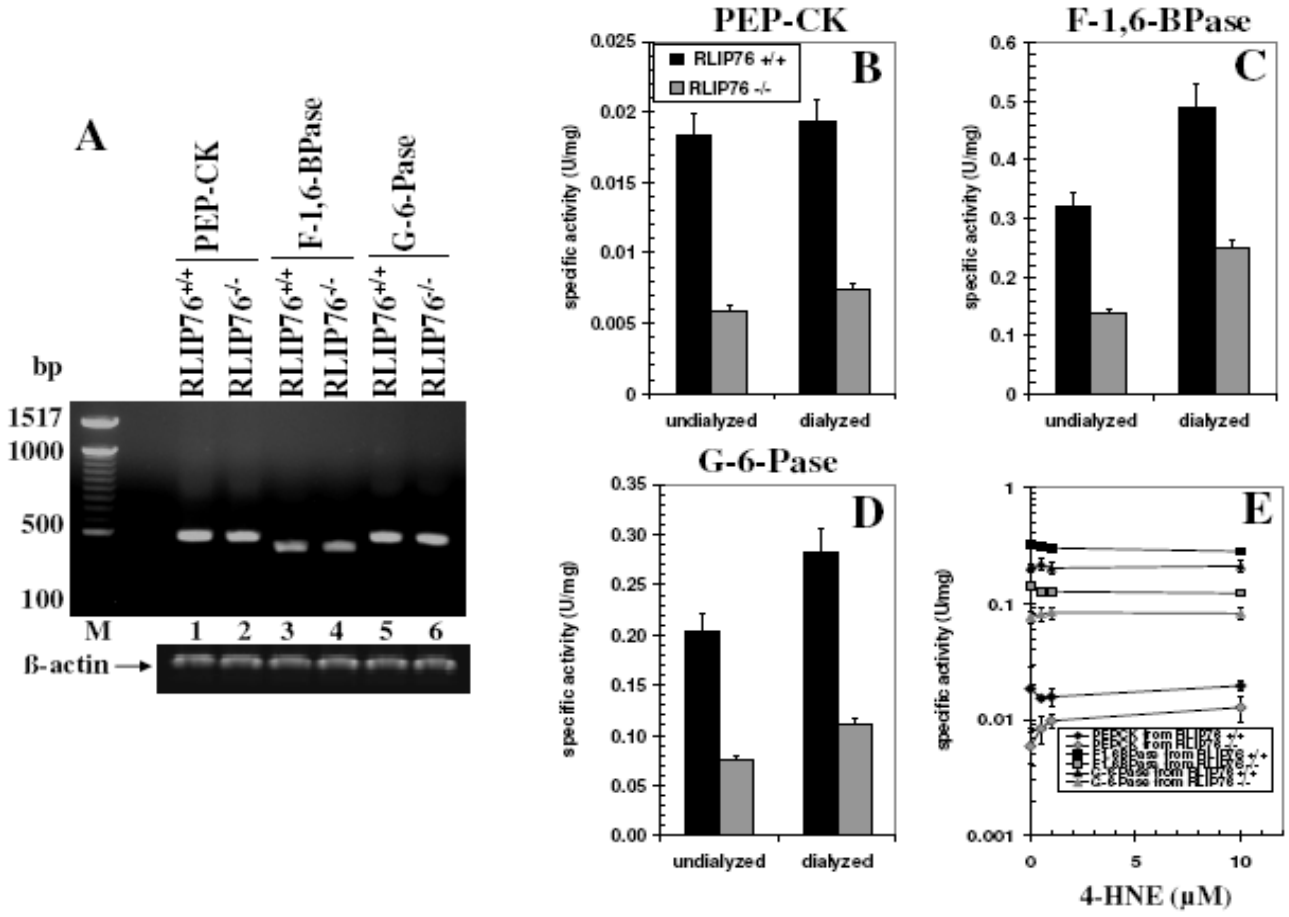

Figure 7

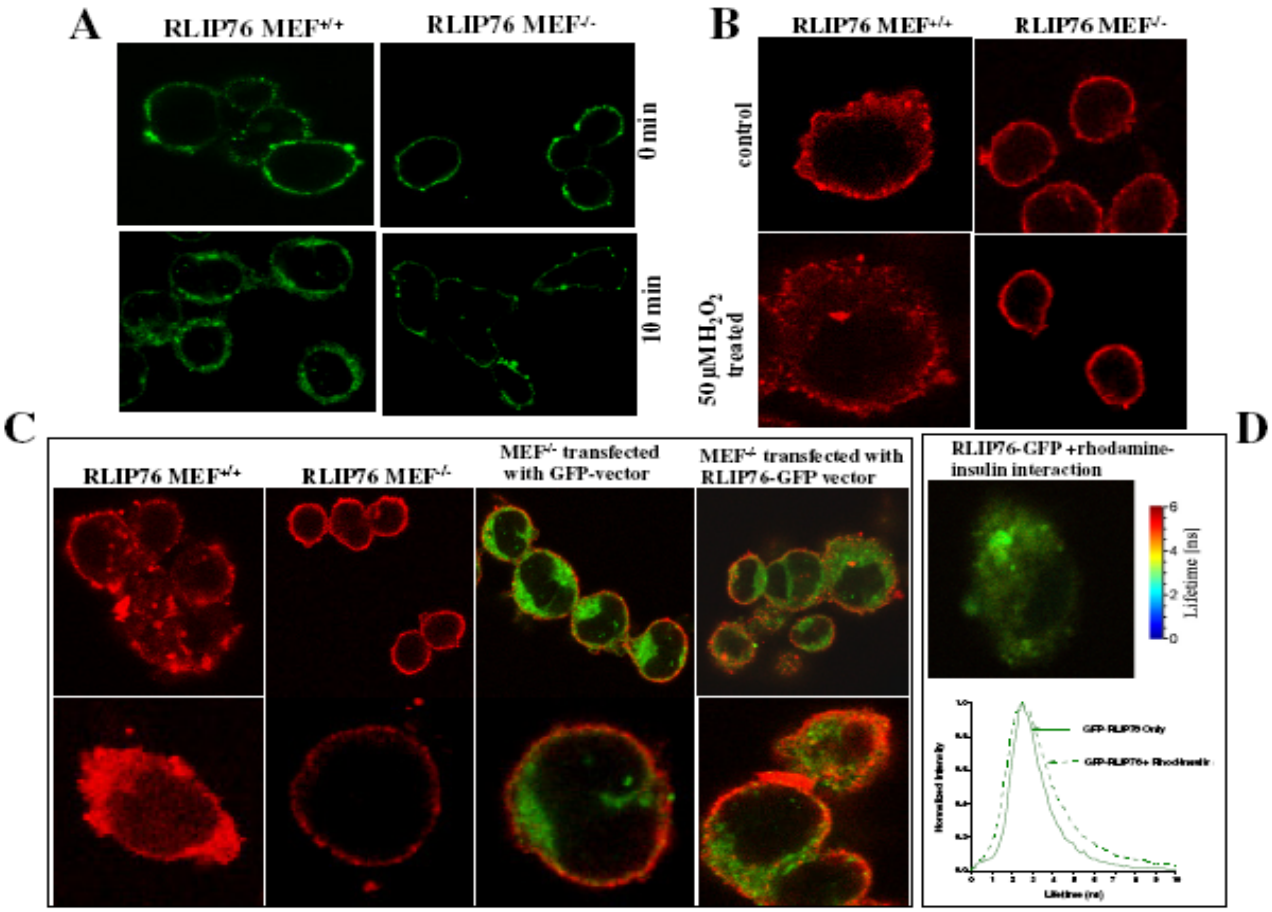
A
RLIP76 MEF+/+
RLIP76 MEF-/-
0 min
10 min
B
RLIP76 MEF+/+
RLIP76 MEF-/-
control
50 μM H2O2 treated
C
RLIP76 MEF+/+
RLIP76 MEF-/-
MEF-/- transfected with GFP-vector
MEF-/- transfected with RLIP76-GFP vector
D
RLIP76-GFP +rhodamine-insulin interaction
Lifetime [ns]
GFP-RLIP76 Only
GFP-RLIP76+ Rhodamine
Normalized Intensity
Lifetime (ns)

Figure 8

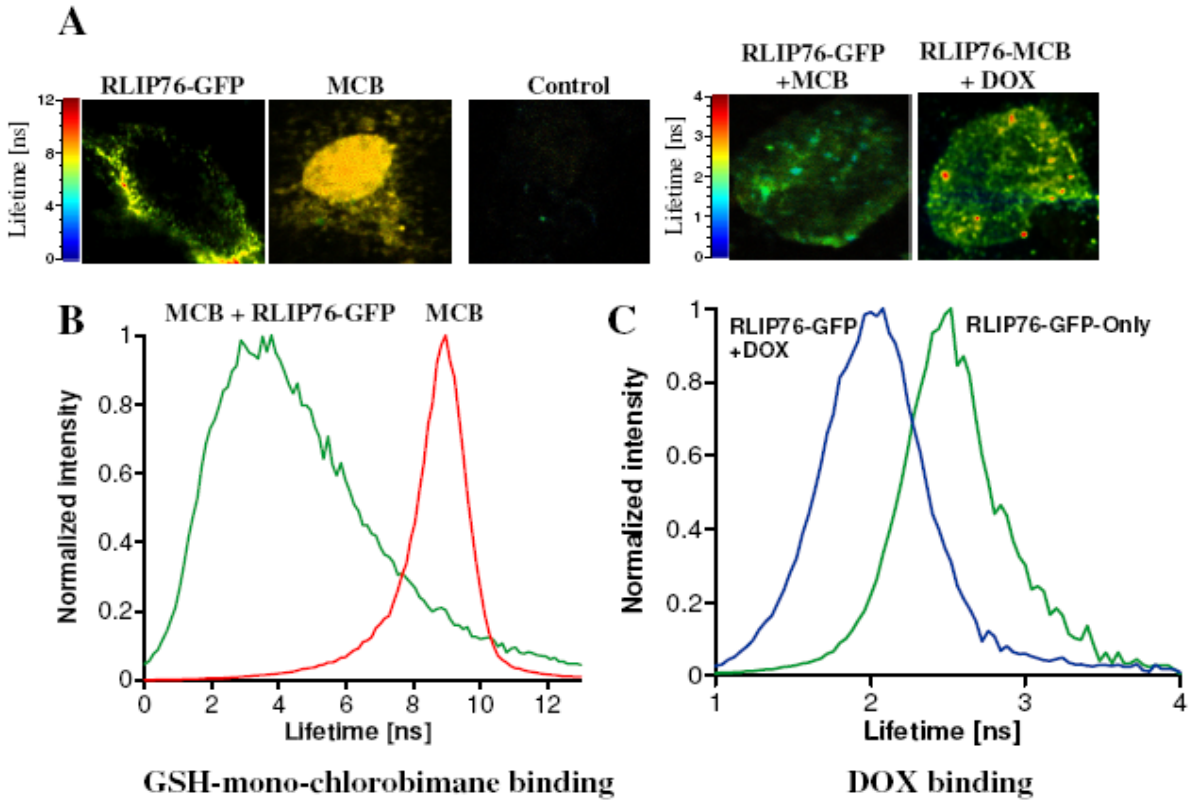
A
RLIP76-GFP
MCB
Control
RLIP76-GFP +MCB
RLIP76-MCB + DOX
Lifetime [ns]
B
MCB + RLIP76-GFP
MCB
Normalized intensity
Lifetime [ns]
GSH-mono-chlorobimane binding
C
RLIP76-GFP +DOX
RLIP76-GFP-Only
Normalized intensity
Lifetime [ns]
DOX binding

Figure 9

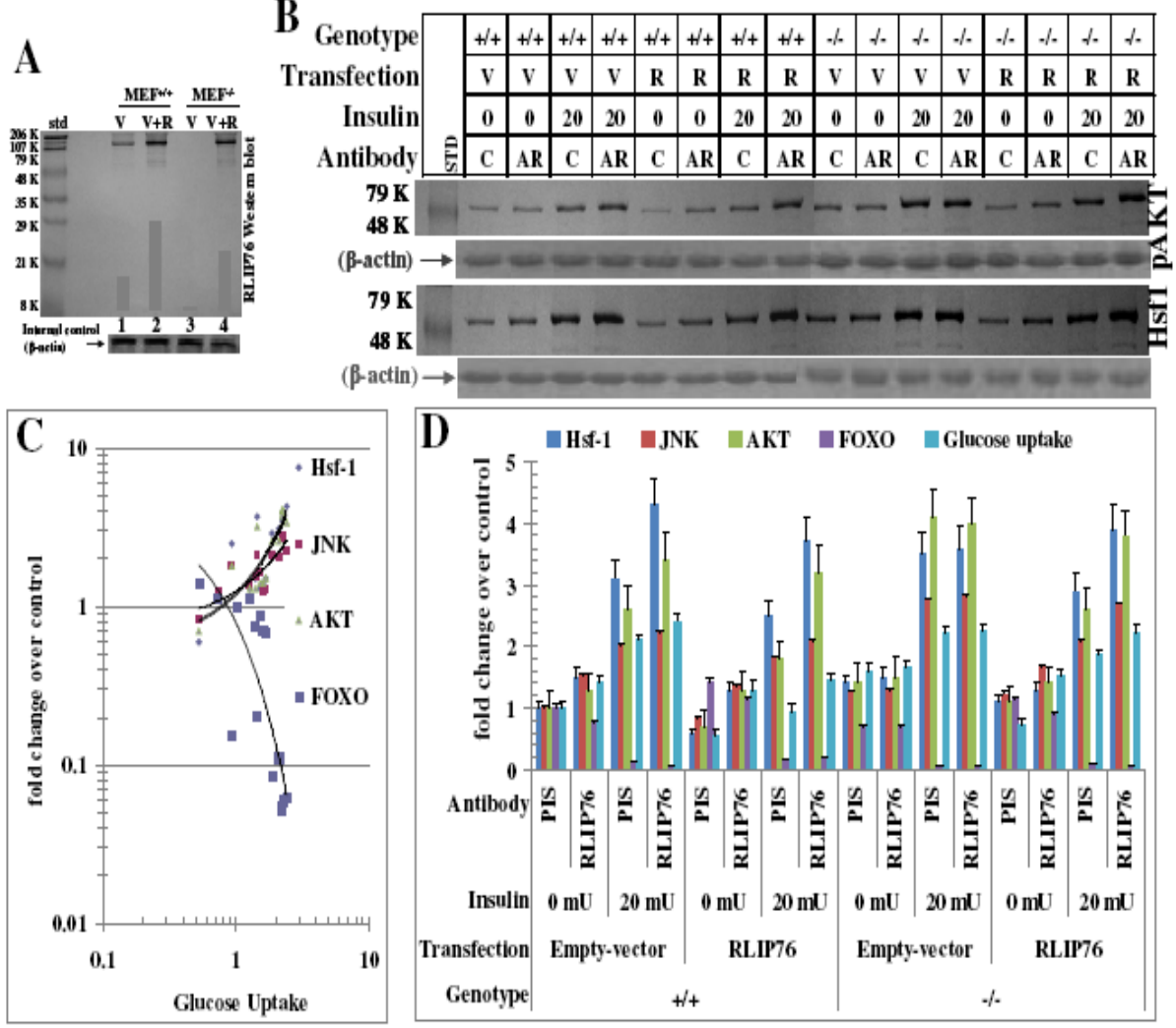
A
std
MEF+/+
MEF-/-
V
V+R
V
V+R
206 K
107 K
79 K
48 K
35 K
29 K
21 K
8 K
RLIP76 Western blot
Internal control
(β-actin)
1
2
3
4
B
Genotype
Transfection
Insulin
Antibody
STD
79 K
48 K
(β-actin)
pAKT
HsfT
C
D
fold change over control
Hsf-1
JNK
AKT
FOXO
Glucose Uptake
Glucose uptake
Antibody
PIS
RLIP76
Insulin
0 mU
20 mU
Transfection
Empty-vector
RLIP76
Genotype
+/+
-/-